Japanese Journal of Applied Physics
Vol. 45, No. 3B, 2006, pp. 1897–1903

High-Speed Atomic Force Microscopy for Studying the Dynamic Behavior of Protein Molecules at Work

Toshio ANDO[1,2,3*], Takayuki UCHIHASHI[1,3], Noriyuki KODERA[1], Atsushi MIYAGI[1], Ryo NAKAKITA[1], Hayato YAMASHITA[1] and Mitsuru SAKASHITA[1]

[1]*Department of Physics, Faculty of Science, Kanazawa University, Kakuma-machi, Kanazawa 920-1192, Japan*
[2]*Frontier Science Research Organization, Kanazawa University, Kakuma-machi, Kanazawa 920-1192, Japan*
[3]*JST/CREST, 4-1-8 Honcho, Kawaguchi, Saitama 332-0012, Japan*

(Received July 3, 2005; accepted November 28, 2005; published online March 27, 2006)

In the quest for the mechanism of protein functions, various key techniques and instruments have been developed. This is an era when scrutinizing a certain protein from various angles is becoming possible through combined knowledge of its structure and function. However, it is necessary to link these different aspects of a protein along a time axis, but no technology is available for tracing a protein in action, at high spatial and temporal resolutions. Atomic force microscopy made it possible for the first time to view a nanometer-scale world in an aqueous environment. In 2001, we developed the first-generation high-speed atomic force microscope (AFM) that could capture moving protein molecules on video at 80 ms/frame. Since then, we have been carrying out various efforts to increase its scan rate as well as to substantially reduce tip–sample interaction force. The reduction in this force is a key to making the high-speed AFM practically useful in life sciences. Various new techniques and devices developed in the past four years have brought the AFM to its second-generation stage. It can now capture weakly interacting protein molecules successively without disturbing their physiological function. Here, we report our efforts made over the past four years, the present capacity of the high-speed AFM, and our preliminary work on the next generation of the instrument. [DOI: 10.1143/JJAP.45.1897]

KEYWORDS: AFM, protein, bio-imaging, dynamics, high-speed AFM

1. Introduction

Proteins perform various sophisticated functions that manmade machines cannot achieve. Various techniques have been developed to study their molecular mechanism. The physiological action of individual protein molecules can be observed using a fluorescence microscope equipped with a high sensitive video camera. NMR and X-ray crystallography enable the determination of the atomic structure of proteins, and the number of structure-determined proteins is rapidly increasing. Genetic engineering enables us to produce arbitrarily recombinant proteins, thereby making it possible to study the molecular mechanism of a protein's activity at the amino acid level. It is now becoming possible to study proteins thoroughly from various angles by combining knowledge of its composition, structure, and function. We need to link these different aspects of protein functions in time. However, information on the nanometer-scale dynamic behavior of proteins has been lacking for a long time.

Atomic force microscopy made it possible for the first time to view a nanometer-scale world in an aqueous environment. Biologists have hoped that it would allow the imaging of the dynamic behavior of protein molecules at work. However, its scan speed is too slow to capture biological processes at the molecular level in real time. Scan speed is determined by the bandwidth of the feedback operator that keeps the tip–sample interaction force constant by moving the sample stage up and down depending on sample height. Since biological samples are soft and fragile, this feedback operation is indispensable for minimizing such interaction force. In this feedback operation, various devices are involved, such as a cantilever, a detector for sensing cantilever deflection, a feedback circuit, and a z-scanner that moves the sample stage in the z-direction. Various efforts have been made to date for the purpose of enhancing feedback speed. Viani *et al.* used small cantilevers with resonant frequencies of 150 kHz to image DNA and GroEL–GroES complexes on mica, in liquid.[1,2] However, their frame rate was less than 1/s, because the conventional piezotube scanner they used had a low resonant frequency in the z-direction. To overcome the low resonant frequency of conventional sample-stage scanners, Sulcheck *et al.*[3,4] and Rogers *et al.*[5] used a cantilever with an integrated zinc oxide piezoactuator capable of deflecting itself to keep the tip–sample interaction force constant. They achieved an imaging rate of $\sim$4/s.[3] However, the self-actuating cantilever inevitably becomes very stiff, and hence is inappropriate for the imaging of soft samples. Although it was performed not with atomic force microscopy (AFM) but rather with near-field scanning optical microscopy, Humphris *et al.* achieved an imaging rate $>$100 frames/s, using a scan system that employs the mechanical resonance of an optical fiber probe to address the sample.[6] However, this high speed is achieved without any feedback operation to keep the probe-sample distance constant. Therefore, this technique is applicable only to the AFM imaging of hard samples. We optimized all the devices involved in the feedback loop, and were able to produce a high-speed AFM that made it possible, in the tapping mode of operation, to capture rapidly moving protein molecules on video at a frame rate of 12.5/s.[7,8]

However, it became clear later that the high-speed AFM could not capture weakly interacting protein molecules, because the protein–protein interaction was largely disturbed by the tip–sample interaction.[9] The difficulty in developing a high-speed AFM for life sciences lies not only in enhancing scanning speed, but also in keeping the tip–sample interaction force small. These two aspects are often contrary to each other. We have been developing various

*E-mail address: tando@kenroku.kanazawa-u.ac.jp

techniques to make these aspects compatible.[9,10] Now the second-generation high-speed AFM can capture weakly interacting proteins on video, without disturbing their physiological action.

2. Quantification of Feedback Bandwidth

Since the tapping mode of operation is most suitable for observing soft samples that are weakly attached to a substratum, here we consider only this mode. The cantilever is oscillated at (or near) its resonant frequency. The oscillating tip briefly taps the surface of the sample at the bottom of each swing, resulting in a decrease in oscillation amplitude. This decrease is used to determine sample height. Sulcheck *et al.* qualitatively analyzed how feedback bandwidth in the tapping mode is affected by various factors, such as the set-point, sample height, resonant frequency and oscillation amplitude of the cantilever.[4] From the qualitative description, we cannot get a prospect of how extensively we have to improve various devices in order to enhance feedback bandwidth. Here, we give a semi-quantitative description.

Suppose that a sample on a substrate has a periodicity λ and that the sample stage is moved horizontally at a velocity V_s, the spatial frequency $1/\lambda$ is converted to a temporal frequency $f \equiv V_s/\lambda$. This is the feedback frequency at which the sample stage is moved in the z-direction. The most rigid definition of feedback bandwidth is the feedback frequency at which feedback operation is phase-delayed at less than 45°. This corresponds to a time delay $1/8f$. The feedback loop contains various delaying steps. The main delays are in the time of reading the cantilever's oscillation amplitude (it takes at least $1/f_c$), (2) the cantilever's response time ($Q_c/\pi f_c$), and (3) the z-scanner's response time ($Q_s/\pi f_s$), where Q_c and f_c are the quality factor and resonant frequency of the cantilever, and Q_s and f_s are the quality factor and resonant frequency of the z-scanner, respectively. These delays and additional delays (the total, Δ) give the following relationship.

$$f < \frac{f_c}{8} \Big/ \left(1 + \frac{Q_c}{\pi} + \frac{Q_s f_c}{\pi f_s} + f_c \Delta\right) \tag{1}$$

Here we have to note that the differential operator of the proportional-integral-differential (PID) feedback circuit can partially compensate the phase delays. Feedback bandwidth is not determined only by eq. (1), but also by sample height (h), the free oscillation amplitude (A_0) of the cantilever, and the setpoint (rA_0). This is because the cantilever tip end tends to detach completely from the sample surface when scanning over a downhill, and its tendency is affected by these factors. Once detached, the tip end cannot re-land on the surface quickly (like "parachuting"), because the error signal is saturated at $(1-r)A_0$. The time required for re-landing is roughly proportional to $\kappa \equiv h/(1-r)A_0$. Therefore, feedback bandwidth is also a function of κ. The condition (as a first approximation) that the oscillating tip should touch even the steepest downhill of sample surface at the bottom of every swing leads to the following relationship.

$$f < \frac{f_c}{\pi} \sin^{-1} \frac{1}{\kappa} \tag{2}$$

Feedback bandwidth is determined by either the smaller term on the right sides of eqs. (1) and (2). Although it is difficult to obtain theoretically a precise analytical expression for feedback bandwidth as a function of various parameters, we can obtain a quantitative expression experimentally. The frame acquisition time (T) is determined by feedback bandwidth (f), the scan size (L), the number of scan lines (N), and the apparent sample size (λ), as shown below.

$$T = 2NL/\lambda f \tag{3}$$

3. New Devices

3.1 Active damping of scanner

The scanner is newly designed, employing a flexure stage instead of the ball-guide stage used in our first-generation high-speed AFM.[7,8] As we reported previously, the structural resonance of the z-scanner is eliminated using two z-piezoactuators placed in the counter direction. The actuators are replaced with customized stack piezoactuators ($3 \times 3 \times 3\,\mathrm{mm}^3$, NEC-Tokin, Tokyo) with a self-resonance frequency of 420 kHz and a maximum displacement of 900 nm (at 100 V). A glass sample stage, which has a circular trapezoid shape with a small top surface of 1 mm diameter, is attached to the top of one of the z actuators via a thin layer of nail enamel. To maintain balance, a dummy stage that has the same mass as the sample stage is attached to the counterbalance z-piezoactuator.[7,8] The open-loop transfer function of the z-scanner is represented by curves (a) in Fig. 1. A resonant peak appeared at approximately 150 kHz, with $Q = 18$. A tiny bump in the gain that appears at approximately 50 kHz is due to the structural resonance of the z-scanner. Without counterbalance (curves b), it appears with a much larger amplitude.

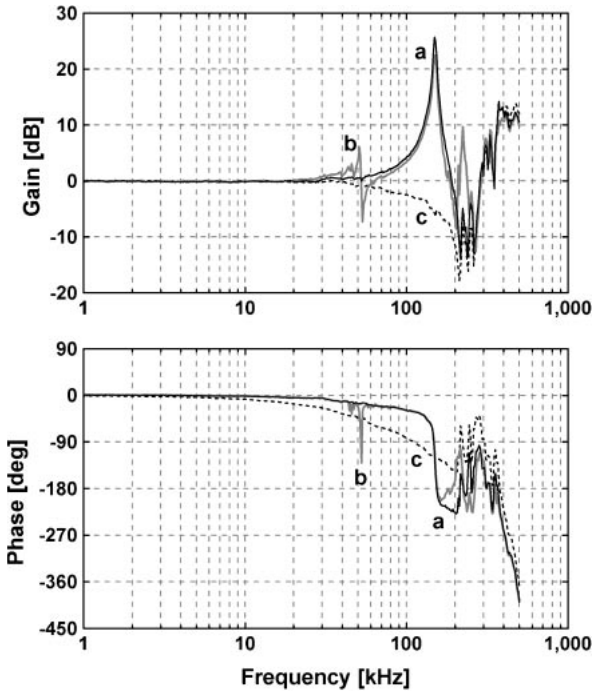

Fig. 1. Open-loop transfer functions of z-scanner (a) without active damping and with counterbalancing, (b) without active damping and counterbalancing, and (c) with active damping and counterbalancing.

The response time of the z-scanner is 38 μs. This slow response is due to the large Q value. When active Q-control is applied to the z-scanner to reduce its Q value, it is necessary to detect the displacement of the z-actuators, which is not easy to do. However, the mechanical response of the z-actuators is well approximated by a second-order transfer function. The input–output relationship is determined only by the transfer function. Therefore, instead of monitoring the displacement of each piezoactuator, we can monitor output signals from a resonant system ("mock" z actuator) which is characterized by the same transfer function as that of the z-piezoactuator.[10] We constructed the mock actuator from a LCR circuit. Using this active Q-control, the Q value of the z-actuators is reduced to 0.5 (curves c), resulting in a 36-fold enhancement in response speed (response time = 1.1 μs).

A drawback is that the phase delay becomes pronounced as shown in Fig. 1 (lower panel). We compensated this delay by means of an inverse transfer function method,[10] and succeeded in extending frequency resulting in a 45° phase delay from 51 to 131 kHz. Because this phase compensation increases the gain in proportion to frequency, higher-order resonant vibrations were increased. We solved this problem by adding more mock z-actuators corresponding to higher-order resonant vibrations, and by using notch filters in series to remove high-frequency noises (>1 MHz).

The same technique applied above to the z-actuators was also used to remove the resonant vibrations of the x- and y-scanners. This resulted in almost no vibrations in the z-direction even when the frame rate was increased up to 30 frames/s.

3.2 Dynamic PID control

For the tapping force to be kept very small, the cantilever's oscillation amplitude has to be kept very close to the free oscillation amplitude. This condition often causes a complete detachment of the cantilever tip from the sample/substratum surfaces. Once detached, re-landing is attained very slowly, just as in "parachuting", because of "feedback saturation" (i.e., the error signal saturates at a low level, independently of how far the tip separates from the surface at the bottom sweep). During parachuting, all information on sample topography is lost. Therefore, the faster the scan is made over a steep-downhill sample surface, the lower the setpoint has to be set to avoid feedback saturation. Feedback saturation also occurs when the tip encounters a steep-uphill sample surface, because cantilever oscillation would be completely quenched in this encounter. This malfunction is more seriously pronounced during faster scanning. Fast scanning would thus not be compatible with harmless scanning.

When the setpoint (rA_0) is very close to the free oscillation amplitude (A_0), the saturated error signal $(1 - r)A_0$ is very small. In addition, the conventional PID controller operates mainly with the integral function. Therefore, the very small saturated error signal prolongs the period of parachuting. The gain parameters of the PID controller can be increased to shorten parachuting period, but this often results in feedback control instability. To overcome this problem associated with the conventional PID, we devised a new PID controller (dynamic PID) that was practically free of feedback saturation.[9] Here, "dynamic" means that the gain parameters of the PID can be changed dynamically depending on tip–sample interaction force. The dynamic PID controller is constructed with a circuit named the *dynamic operator*, which is inserted between the error signal and the input of a conventional PID circuit. This dynamic operator works as follows (Fig. 2). A threshold level (A_{upper}) is set between rA_0 and A_0. When the cantilever oscillation amplitude (A) exceeds A_{upper}, the differential signal $A - A_{\mathrm{upper}}$ is amplified and added to the error signal. The error signal that now contains an extra signal is fed to the conventional PID. This "false error signal", which is larger than the "true error signal", produces a quicker feedback action, thereby A quickly becomes smaller than A_{upper}, and then feedback operation returns to the conventional one. By these actions, the feedback does not practically saturate even when the true error signal saturates at a low level. A similar manipulation of the error signal can also be made when A is smaller than rA_0. In this case, a new threshold level (A_{lower}) is set lower than rA_0 (Fig. 2). When A becomes smaller than A_{lower}, the differential signal $A - A_{\mathrm{lower}}$ is amplified and added to the true error signal. This manipulation can keep the cantilever tip from pushing against the sample too strongly, especially when the tip encounters a steep-uphill surface of the sample.

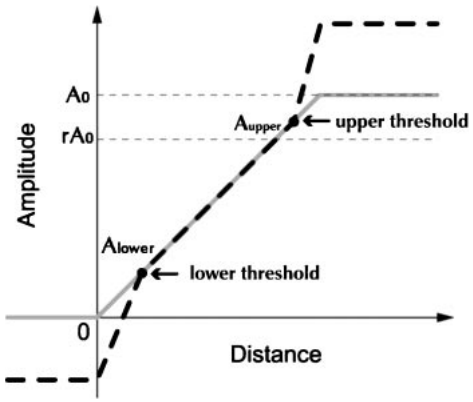

Fig. 2. Schematic of dynamic PID control technique. The gray line represents the amplitude–distance curve. The broken line indicates a false amplitude–distance curve produced when dynamic PID control operates.

The feedback performance of the dynamic PID controller was compared with that of the conventional PID controller, using a mock sample surface consisting of four rectangular steps with two different heights: one height is equal to A_0, and the other is 2 times higher than A_0. The scan speed is 0.25 mm/s, and the setpoint is $0.9 \times A_0$. With the conventional PID controller, the topographic image is very blurred, because of a long period of parachuting [Fig. 3(a)]. On the other hand, with the dynamic PID controller, the image is very clear, indicating that there is no complete detachment of the cantilever tip from the sample surface [Fig. 3(b)]. Next, the closed loop feedback bandwidth was measured as a function of setpoint level. In this measurement, the sample stage height was varied using sinusoidal wave signals, and the PID output signal was monitored. With the conventional PID controller, feedback bandwidth is gradually decreased with increasing setpoint level from $0.7A_0$ to $0.95A_0$. The bandwidth at $r = 0.95$ is about one-sixth the bandwidth at $r = 0.7$. However, with the dynamic PID controller, the

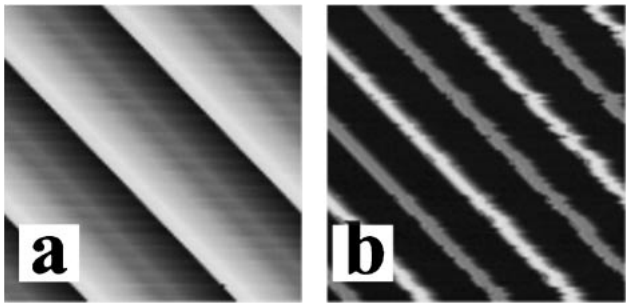

Fig. 3. Effect of dynamic PID control on suppression of parachuting landing of cantilever tip onto surface. AFM images obtained (a) with a conventional PID controller, and (b) with the dynamic PID controller.

bandwidth is almost constant, irrespective of setpoint level. Thus, the dynamic PID control is a superior technique enabling the fast-scanning tip to touch samples very lightly.

3.3 Cantilevers

The small cantilevers that we developed together with Olympus in 2001 had a resonant frequency of 600 kHz in water, and a spring constant of approximately 150 pN/nm.[7] Since the lever did not have a probe tip, the tip had to be grown using electron beam deposition (EBD). Recently, Olympus has developed smaller cantilevers integrated with beaklike tips [Fig. 4(a)].[11] The resonant frequency was 800 kHz–1.2 MHz in water, and the spring constant ranged from 100 to 250 pN/nm. Although we still have to grow an EBD tip on a beaklike tip, a much shorter EBD tip is sufficient [Fig. 4(b)], compared with that on the previous flat levers.

3.4 Other devices

Although not completed yet, here, we briefly mention how we have been working toward the third-generation high-speed AFM. To enhance feedback bandwidth, it is important to increase the resonant frequency of the *z*-scanner, but available piezoactuators with enough displacement are limited in the resonant frequency. We estimate that the achievable maximum resonant frequency of a piezo-stage scanner will be limited to be about 300 kHz, only twice that of our *z*-scanner. Self-actuating cantilevers are an alternative to the piezo-stage scanner,[3–5] but a cantilever with an integrated zinc oxide piezoactuator inevitably becomes too stiff. Driving a cantilever coated with a thin magnetic film directly by a magnetic field is also an alternative.[12] However, a magnetic-film coating sufficient for the cantilever to be driven reduces the resonant frequency of the cantilever. To drive a cantilever by a different means, we measured the cantilever deflection caused by the photothermal expansion of gold coated onto a Si_3N_4 cantilever surface. The sensitivity was about 10 nm/mW in an aqueous solution, when a 405 nm violet laser was used with our small cantilevers. Because of the slow heat transmission, the response time of the deflection was about 30 μs. However, inverse transfer function compensation was apparently able to eliminate the slow heat transmission. Since the maximum displacement of the cantilever driven by photo-thermal expansion has been limited so far, and the "cantilever scanner" requires a large dynamic range of the deflection detection sensor (which reduces sensor sensitivity), it is apparent that this technique has to be used together with the conventional piezo-stage scanner. Photo-thermal expansion can also be use to directly excite a cantilever at its resonant frequency.[13] Unlike acoustic excitation, it does not have the "forest-of-peaks" effect. This superior attribute facilitates the active control of the cantilever to reduce Q value, which enhances the response speed of the cantilever (and hence feedback bandwidth). Another device that we have been trying to include in the third-generation high-speed AFM is a feed-forward controller.[14] Topographic differences between two adjacent line scans are not large, as long as the sample is moving slowly. Therefore, line-by-line feed-forward control can facilitate performance of the feedback-control task. Using stationary samples, we confirmed that a significant extension of feedback bandwidth was achieved by the feed-forward control. However, when the sample is moving quickly, the feed-forward control is supposed to act occasionally in an undesirable direction. Yet, we have not noticed an ill effect expected from such an undesirable action even with rapidly moving samples. This may be due to the small time difference (less than 1 ms) between two line scans.

4. Bioimaging

In our first-generation high-speed AFM, the tip–sample interaction force was too large to image fragile protein

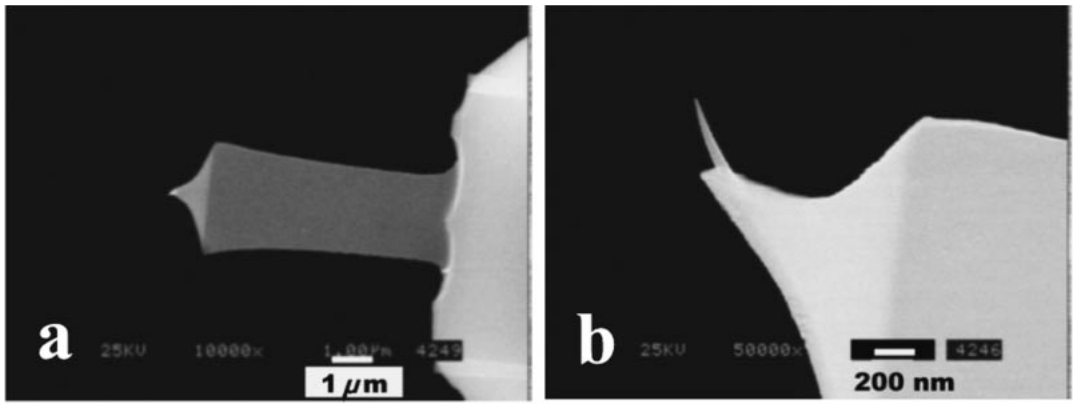

Fig. 4. Electron micrographs of small cantilever with beaklike tip (a) without an EDB tip, and (b) with an EBD tip grown on beaklike tip.

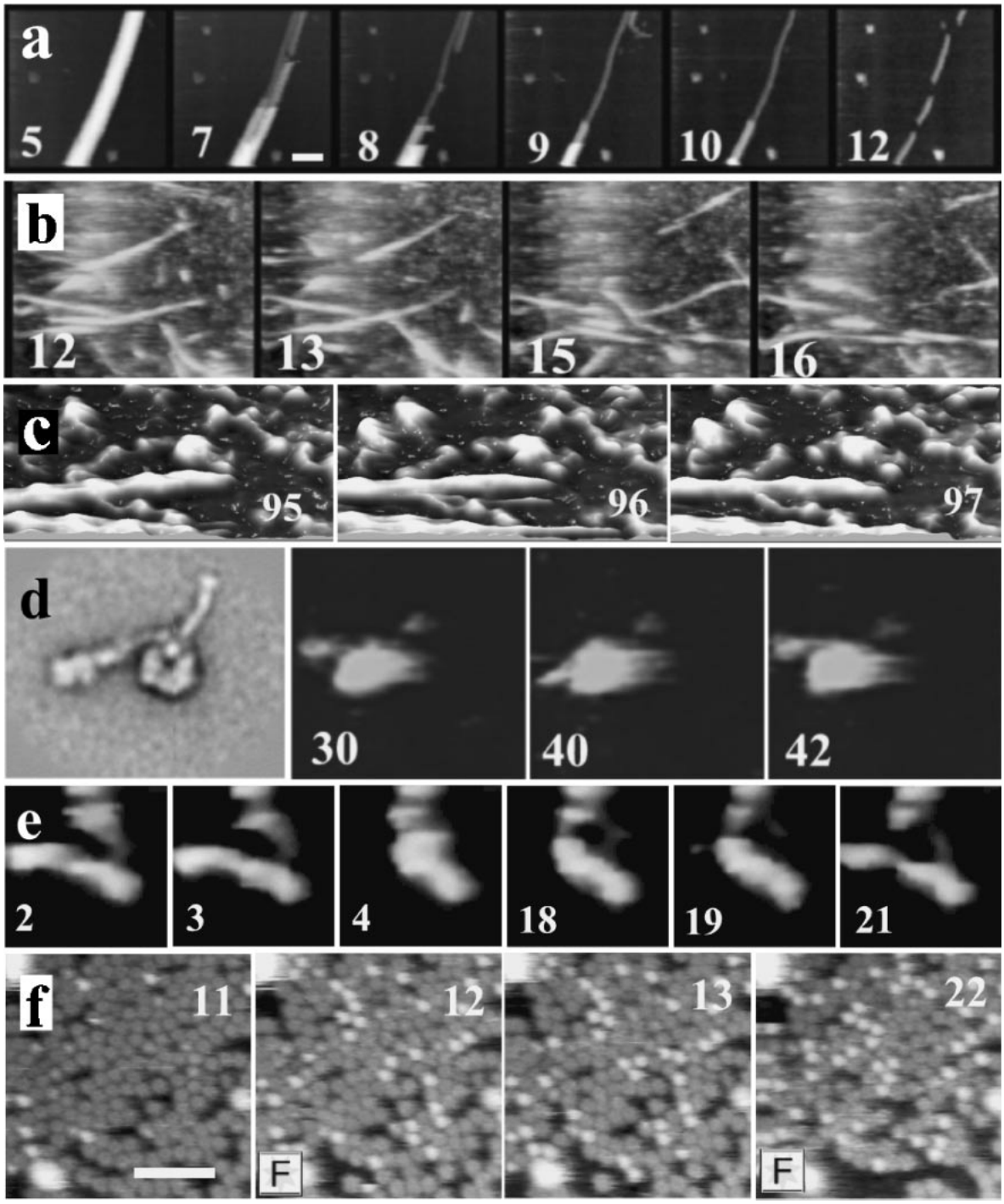

Fig. 5. Successive AFM images of biological samples captured using high-speed AFM. All the numbers indicate frame numbers. (a) Microtubules being destroyed during imaging (scale bar, 100 nm; 640 ms/frame), (b) actin filaments gliding over myosin V-coated surface (scan range, 1 μm; 1 s/frame), (c) 3D images of myosin V molecules pulling actin filament leftward (note that the right distal end of the actin filament is moving leftward; 180 ms/frame), (d) dynein C changing its stem orientation during ATPase reaction (160 ms/frame; the most left-hand image is an electron micrograph[15] of dynein C), (e) myosin V changing its conformation after ATP is released from caged ATP by flash photolysis (the UV flash is applied between the third and fourth frames, 80 ms/frame), and (f) GroES binding to GroEL layer after flash-photolysis of caged ATP ("F" denotes that the UV flash is applied just prior to the frames; scale bar, 100 nm; 1 s/frame).

assemblies such as microtubules and actin filaments.[9] These samples were gradually disassembled during imaging [Fig. 5(a)]. Our efforts made to solve this problem led to the new active damping method and the dynamic PID controller, as mentioned above. Owing to these devices, it became possible not only to image fragile samples without disassembly, but also to capture weakly interacting protein molecules without disturbing their physiological functions. This is demonstrated by imaging actin filaments moving, in the presence of ATP, over a surface that is densely coated with myosin V molecules [Fig. 5(b)]. The velocity of actin filaments gliding was very similar to that observed by fluorescence video microscopy. To view the dynamic behavior of individual myosin V molecules when they are

propelling actin filaments unidirectionally, the surface was sparsely coated with myosin V. A short actin filament entirely within the imaging region was observed. This fortunate situation enabled us to identify which myosin V molecules are propelling the actin filament. Two myosin V molecules were interacting with the short actin filament, and only one of the two heads of each myosin V molecule was attached to the actin filament. The actin filament moved leftward in a stepwise manner; the step size was 36 nm, which corresponds to one half of the long helical repeat of an actin filament. During the stepwise movement, the interacting heads did not seem to change their conformations largely [Fig. 5(c)], which was not the behavior expected from the well-studied swinging-lever arm hypothesis in which a large swinging movement of the myosin's neck domain is supposed to propel an actin filament.

Dynein C is a single-headed dynein. A stalk and a stem are protruded from the ring-shaped head, and the stalk interacts with microtubules at its globular distal end. Electron micrographs of dynein C revealed that the angle between the stalk and the stem differed between the apo state (no-nucleotide) and the ADP-Vi bound state.[15] The nucleotide-dependent change in the structure is hypothesized to drive microtubule movement. However, ADP-Vi is a non-natural substrate, and therefore it is not certain that such a change in angle really occurs during the ATPase cycle. High-speed AFM imaging of dynein C in the presence of ATP revealed that it does certainly occur [Fig. 5(d)]. The stalk and head seemed stationary, but the stem went back and forth between two positions. The stem-stalk angle changed between 137 and 184°; the former angle corresponds to the apo state, and the latter was larger than that of the ADP-Vi bound state (159°). The frequency of the change in angle approximately coincided with the ATPase rate. Therefore, it is very certain that the stem movement observed is driven by the ATPase reaction. This is the first time that a cyclic protein's conformational change has been captured on video in real time.

The ATPase rate of dynein C is relatively high. However, the ATPase rate of myosin V is very low, about 0.05/s.[16] It is thus difficult to capture cyclic conformational changes in myosin V during the ATPase reaction. To facilitate such an observation, we introduced a UV photolysis system to the AFM; ATP is quickly released from caged ATP upon UV light application.[17] As shown in Fig. 5(e), myosin V bent at the head-neck junction immediately after UV irradiation, and then returned to the original straight form. This technique is very valuable for recording substrate-induced conformational changes in proteins, because protein molecules weakly attached to the substratum are always moving due to thermal agitations, therefore, in steady-state recording, it is not easy to distinguish Brownian movement from the substrate-induced conformational change.

The UV photolysis of caged ATP was applied to the GroEL–GroES system. GroEL is a chaperonin that assists its substrate polypeptides to fold into their functional three-dimensional (3D) structures, and GroES is a co-chaperonin. GroEL consists of two homo-heptameric rings that are stacked back to back,[18] whereas GroES is a single homo-heptameric ring.[19] GroES binds to GroEL only when GroEL is in the nucleotide-bound state. GroEL was attached to the mica surface with an end-up orientation, forming a highly packed single layer [Fig. 5(f)]. The central channel of the GroEL ring was therefore visible. Before UV application, GroES was floating in the solution containing caged ATP, and therefore not visible. High-frequency pulses of a UV laser light (355 nm) were applied within 5 ms while y-return scanning was performed. Immediately after this, GroES attached to the top of GroEL, forming protrusions on the GroEL layer. Since the concentration of the ATP produced in the small UV-irradiated volume quickly decreased due to diffusion, the second application of UV pulses resulted in more protrusions. Using this technique, the nucleotide-induced *cis–trans* conformational transition of individual GroEL molecules was also studied.[20]

5. Discussion

Our second-generation high-speed AFM has the capacity to dissect dynamic processes of individual protein molecules at work. The compatibility of a high scan rate and a skimming scan over fragile samples is successfully achieved. Scan rate has reached a level at which video-rate imaging is nearly possible. Tip–sample interaction force is greatly reduced to a level where it does not disturb weak protein–protein interactions. The active damping that we have developed for the sample-stage scanner[10] is widely applicable, not only to any type of scanning probe microscope, but also to instruments where fast and precise mechanical displacement is required. The dynamic PID operator we have developed is realized with a simple analogue circuit, and hence works very fast. Various types of robust feedback techniques have been proposed,[21,22] and the usefulness of some of them has been demonstrated with conventional AFMs. However, most of them require intricate calculations by a computer or a DSP system, and even with a fast computer/DSP, the required calculation time seems to be too long for digital feedback operators to be implemented in the high-speed AFM.

What new developments will the next generation high-speed AFM for life sciences require? The cantilever and z-scanner are devices that must be improved to achieve a higher scan rate. At present, their respective response speeds are similar to each other, because the cantilever's Q value cannot be reduced from its natural Q value in water ($\sim$2.0) due to the lack of means to excite the cantilever directly. This is one reason we have recently been trying to use the photo-thermal actuation of a cantilever. We are now developing smaller cantilevers with a resonant frequency of 2 MHz in water. When such cantilevers are combined with photo-thermal actuation to excite their resonance with active damping as well as to deflect them to control tip–sample distance, feedback bandwidth will reach $\sim$200 kHz. This bandwidth will enhance the frame rate up to 40–50 frame/s (with the scan size of $\sim$250 nm). The line-by-line feed-forward control will become more useful for observing moving proteins, when a higher scan rate is available. The higher the scan rate the smaller are the height changes produced by the movement during the time interval of two adjacent line scans. By adding the feed-forward control to the above-mentioned improvements, we may be able to reach a frame rate of $\sim$100 frames/s. Not only changes in protein shapes, but also a change in the map of their

physicochemical properties, such as electrostatic properties, are involved in proteins' physiological functions. AFM can map such properties in the non-contact phase-imaging mode.[23,24] Small cantilevers for high-speed imaging have a large resonant frequency as well as a small spring constant. These mechanical properties sensitize phase detection markedly. Therefore, in phase detection, we do not have to rely on a large Q value of the cantilever and slow phase-measurement instruments. This will enable high-speed phase imaging in the near future.

The observation of the nanometer-scale dynamic behavior of protein molecules in action has just been started recently. Numerous biological processes are waiting to be imaged by the high-speed AFM, such as processive motors moving along their tracks, molecular chaperones assisting a polypeptide chain to fold, and a ribosome synthesizing a polypeptide according to the nucleotide sequence on mRNA. In addition, the not-yet-studied subject of how proteins dynamically change their physicochemical properties while functioning is waiting to be studied. Together with the knowledge attainable from established techniques, the protein dynamics that will be revealed for the first time by the high-speed AFM will uncover the molecular mechanisms of protein functions.

Acknowledgement

This work was supported by CREST/JST, Special Coordination Funds for Promoting Science and Technology (Effective Promotion of Joint Research with Industry, Academia, and Government) from JST, and a Grant-in-Aid for Basic Research (S) from the Ministry of Education, Culture, Sports, Science and Technology of Japan.

1) M. B. Viani, T. E. Schäffer, G. T. Paloczi, L. L. Pietrasanta, B. L. Smith, J. B. Thompson, M. Richter, M. Rief, H. E. Gaub, K. W. Plaxco, A. N. Cleland, H. G. Hansma and P. K. Hansma: Rev. Sci. Instrum. **70** (1999) 4300.
2) M. B. Viani, L. I. Pietrasanta, J. B. Thompson, A. Chand, I. C. Gebeshuber, J. H. Kindt, M. Richter, H. G. Hansma and P. K. Hansma: Nat. Struct. Biol. **7** (2000) 644.
3) T. Sulchek, R. Hsieh, J. D. Adams, S. C. Minne, C. F. Quate and D. M. Adderton: Rev. Sci. Instrum. **71** (2000) 2097.
4) T. Sulchek, G. G. Yaralioglu, C. F. Quate and S. C. Minne: Rev. Sci. Instrum. **73** (2002) 2928.
5) B. Rogers, T. Sulchek, K. Murray, D. York, M. Jones, L. Manning, S. Malekos, B. Beneschott, J. D. Adams, H. Cavaozs and S. C. Minne: Rev. Sci. Instrum. **74** (2003) 4683.
6) A. D. L. Humphris, J. K. Hobbs and M. J. Miles: Appl. Phys. Lett. **83** (2003) 6.
7) T. Ando, N. Kodera, E. Takai, D. Maruyama, K. Saito and A. Toda: Proc. Natl. Acad. Sci. U.S.A. **98** (2001) 12468.
8) T. Ando, N. Kodera, D. Maruyama, E. Takai, K. Saito and A. Toda: Jpn. J. Appl. Phys. **41** (2002) 4851.
9) T. Ando, N. Kodera, Y. Naito, T. Kinoshita, K. Furuta and Y. Y. Toyoshima: ChemPhysChem **4** (2003) 1196.
10) N. Kodera, H. Yamashita and T. Ando: Rev. Sci. Instrum. **76** (2005) 053708.
11) M. Kitazawa, K. Shiotani and A. Toda: Jpn. J. Appl. Phys. **42** (2003) 4844.
12) W. Han, S. M. Lindsay and T. Jing: Appl. Phys. Lett. **69** (1996) 4111.
13) D. Kobayashi, S. Kawai and H. Kawakatsu: AIP Conf. Proc. **696** (2003) 180.
14) G. Schitter, F. Allgöwer and A. Stemmer: Nanotechnology **15** (2004) 108.
15) S. A. Burgess, M. L.Walker, H. Sakakibara, P. J. Knight and K. Oiwa: Nature **421** (2003) 715.
16) T. Sakamoto, I. Amitani, E. Yokota and T. Ando: Biochem. Biophys. Res. Commun. **272** (2000) 586.
17) S. R. Adams and R. Y. Tsien: Ann. Rev. Physiol. **55** (1993) 755.
18) K. Braig, Z. Otwinowski, R. Hegde, D. C. Boisvert, A. Joachimiak, A. L. Horwich and P. B. Sigler: Nature **371** (1994) 578.
19) J. F. Hunt, A. J. Weaver, S. J. Landry, L. Gierasch and J. Deisenhofer: Nature **379** (1996) 37.
20) M. Taniguchi, D. Yamamoto and T. Ando: in preparation.
21) G. Scitter, R. W. Stark and A. Stemmer: Ultramicroscopy **100** (2004) 253.
22) S. Salapaka, A. Sebastian, J. P. Cleveland and M. V. Salapaka: Rev. Sci. Instrum. **73** (2002) 3232.
23) U. Dürig, H. R. Steinauer and N. Blanc: J. Appl. Phys. **82** (1997) 3641.
24) R. Garcia, J. Tamayo and A. San Paulo: Surf. Interface Anal. **27** (1999) 312.